X-ray Sources and Star Formation Activity in the Sgr B2 Cloud Observed with *Chandra*

Shin-ichiro Takagi, Hiroshi Murakami and Katsuji Koyama
Department of Physics, Faculty of Science, Kyoto University, Sakyo-ku, Kyoto 606-8502, Japan;
takagi9@cr.scphys.kyoto-u.ac.jp, hiro@cr.scphys.kyoto-u.ac.jp, koyama@cr.scphys.kyoto-u.ac.jp

ABSTRACT

We report the X-ray population study in the giant molecular cloud Sagittarius B2 (Sgr B2). More than a dozen of X-ray cloud members (and candidates) are discovered with *Chandra*. Two bright X-ray sources are located near Sgr B2 Main, the most copious complex of the ultra compact HII sources. The X-ray spectra are fitted with a thin thermal plasma model of 5–10 keV temperature. The intrinsic luminosity after correcting the absorption of $\sim 5 \times 10^{23}$ H cm^{-2} is $\sim 10^{33}$ erg s^{-1}. Although these two X-ray sources are attributable to young stellar objects (YSOs) in the same HII complex, they are in sharp contrast; one at the center of the HII complex exhibits strong K-shell transition lines of iron, while the other near the east has only weak lines. The other HII complexes, Sgr B2 North and South, also show hard and highly absorbed X-ray emissions due possibly to the star formation activity.

The composite X-ray spectrum of the other cloud member X-ray sources is fitted with a thin thermal plasma of ∼10-keV temperature with the hydrogen column density ($N_{\rm H}$) of 1.3×10^{23} H cm^{-2}, and the individual X-ray luminosity of a few times of 10^{31-32} erg s^{-1}. These are likely to be a single or cluster of YSO(s), but neither radio nor infrared counterpart is found. An alternative scenario of isolated white dwarfs powered by the Bondi-Hoyle accretion from the dense cloud gas is also discussed. The X-ray spectra exhibit an additional 6.4-keV line of neutral or low-ionization irons, which indicates that the environment gas is concentrated near at the sources.

Subject headings: Galaxy: center — ISM: clouds — ISM: individual (Sagittarius B2)— stars: formation — X-rays: individual (Sagittarius B2)— X-rays: stars — X-rays: spectra

1. Introduction

The giant molecular cloud Sgr B2, located at the projected distance of ∼100 pc from the Galactic center (GC), is one of the richest star forming regions (SFRs) in our Galaxy. Due to its proximity to the GC, Sgr B2 is heavily obscured in the optical, even near infrared (NIR) and soft X-ray bands. Accordingly, the star formation activity has been traced mainly with the radio and mid–far infrared (MIR and FIR) bands. The VLA continuum observations have revealed at least 12 separate HII regions in the Sgr B2 cloud (Benson & Johnston 1984), which are grouped into three main concentrations, Sgr B2 North (HII region K), Main (HII regions A–G, I, and J) and South (HII region H). The follow-up high-resolution continuum observations have revealed nearly 60 ultra compact (UC) HII regions lying along the north-to-south elongation (Gaume et al. 1995; De Pree, Goss, & Gaume 1998), which are also traced by molecular lines and FIR (e.g. Sato et al. 2000; Goldsmith et al. 1992). Clusters of molecular maser sources are found from the HII complexes, Sgr B2 North (N), Main (M), and South (S) (H_2O: Kobayashi et al. 1989; OH: Gaume & Glaussen 1990; SiO: Mehringer, Goss, & Palmer 1994; Shiki, Ohishi, & Deguchi 1997). The ages of Sgr B2 (N) and Sgr B2 (M) are estimated to be $\sim 10^4$ years, using the photon flux of the exciting stars and the ambient gas density (De Pree et al. 1995,

1996). Powerful bipolar outflows are found from Sgr B2 (N) and Sgr B2 (M), with the dynamical age of $\sim 10^4$ years (Vogel, Genzel, & Palmer 1987; Lis, et al. 1993; Mehringer 1995; Kuan & Snyder 1996; Liu et al. 1998). MIR sources are also found at Sgr B2 (M) and (S) (Egan et al. 1999). All these results indicate that Sgr B2 harbors many clusters of very young stellar objects (YSOs) of high-mass stars.

There is mounting evidence that star forming regions, whatever low-mass or high-mass, generally emit fairly strong X-rays (e.g., Feigelson & Montmerle 1999 and references there in; Garmire et al. 2000). *ASCA* and later *Chandra* revealed that a significant fraction of YSOs emit hard X-rays above 2 keV (e.g., Koyama et al. 1996a; Shultz et al. 2001; Kohno, Koyama. & Hamaguchi 2002). The hard X-rays can penetrate through the large Galactic $N_{\rm H}$ to Sgr B2, hence may provide a new view on the star formation activity in this cloud. This paper reports on the first *Chandra* results of hard X-ray sources and studies the X-ray population in Sgr B2.

Throughout this paper, the distance to Sgr B2 is assumed to be 8.5 kpc, the same as to Sgr A*, and is similar to the estimated distance of 7.1 $\pm$ 1.5 kpc (Reid et al. 1988).

2. Observations and Analyses

2.1. Source Detection and Identification

The *Chandra* ACIS observation of Sgr B2 was carried out on 29–30 March 2000 with the nominal aim-point at R.A. (2000) = $17^{\rm h}47^{\rm m}07^{\rm s}$, Dec. (2000) = $-28^{\rm d}26^{\rm m}29^{\rm s}$. The satellite and instrument are described by Weisskopf, O'dell, & van Speybroeck (1996) and Garmire, Nousek, & Bautz (2001), respectively. Sgr B2 lies near the center of the ACIS-I array of four front-side illuminated CCDs, each with 1024×1024 array of $0''.5 \times 0''.5$ pixels covering a $8' \times 8'$ field of view. Using the Level 2 processed events provided by the pipeline processing at the *Chandra* X-ray Center, we selected the *ASCA* grades[1] 0, 2, 3, 4, and 6, as X-ray events; the other events, which are due to charged particles, hot and flickering pixels, are removed. The effective exposure is about 100 ksec.

In the soft (0.5–2.0 keV) band image of the ACIS-I field of $17'.4 \times 17'.4$, we find four bright X-ray sources that have *Tycho-2* counterparts. The positions of the *Tycho-2* sources have accuracy of 60 mas (Høg et al. 2000), hence the *Chandra* frame is fine-tuned using these four sources within an absolute error of 0.25 arcsec (1 sigma dispersion). In order to search the Sgr B2 cloud member sources, we run the program of *wavdetect* [2] in the 2–10 keV band, because X-ray photons below 2 keV are totally absorbed by the interstellar gas to Sgr B2 of $\sim 1 \times 10^{23}$ H cm^{-2} (Sakano 2000). The threshold significances of the *wavdetect* are set at 10^{-6} and 0.001 for the source list and the background estimation, respectively. The wavelet scales are 1, $\sqrt{2}$, 2, $2\sqrt{2}$, 4, $4\sqrt{2}$, 8, $8\sqrt{2}$, and 16 pixels. We then find 15 sources in the Sgr B2 cloud area of a $3' \times 3'.5$ region.

The 2–10 keV band image of this region and the position of detected X-ray sources are given in Figure 1 by the solid circles with a diameter of three times of the half power diameter (HPD) of the point spread function (hereafter, 3×HPD). In addition to the *wavdetect* search, we inspect X-ray sources manually from all the compact HII regions including the Sgr B2 (N) and (S) complexes. For this search, we extract the X-ray photon from a 3×HPD-diameter circle or from the same area as the HII regions (those extending larger than 3×HPD). We then find X-ray excess from Sgr B2 (N) and Sgr B2 (S) with more than 3σ confidence level (in the 2–10 keV band). The source areas are also given by the dotted box (Sgr B2 (N)) and circle (Sgr B2 (S)) in Figure 1. Since this paper focuses on single or compact cluster of point sources, we do not search diffuse sources other than those of the HII regions. All the detected sources, the positions and photon counts are listed in Table 2.

The closed-up image of Sgr B2 (M) is shown in Figure 2 overlaid on the radio contours. The brightest X-ray sources in Sgr B2, No. 10 and 13 are located in this complex.

2.2. Spectrum and Time Variability

The X-ray spectra are made from the source areas given in Figures 1 and 2. In order to properly subtract the diffuse X-rays in the Sgr B2 and GC regions (Murakami, Koyama, & Maeda 2001;

[1] see http://asc.harvard.edu/udocs/docs/POG/MPOG/index.html

[2] see http://asc.harvard.edu/udocs/docs/swdocs/detect/html/

Koyama et al. 1996b), we make the background spectrum from the full region of Sgr B2 excluding all the source areas (see Figure 1). Since No. 10 and 13 are located in the local diffuse maximum near the HII complex Sgr B2 (M) (Murakami et al. 2001), the background data are taken from a $30''$-radius circle with the center at the middle of the two sources (the data in the source regions are excluded). No. 16, on the other hand, lies in a local diffuse minimum, hence the background is taken from an annulus around the source.

To eliminate obvious foreground or background sources, the background-subtracted spectra are fitted with a model either power-law of fixed photon indices 2.0, or 1-keV thin thermal plasma of solar-abundances; the former is representative to background AGNs and the latter is for foreground stars. The interstellar $N_{\rm H}$ to Sgr B2 is $\sim 10^{23}$ H cm^{-2} (Sakano 2000), while that of intra-Sgr B2 cloud is $\sim 10^{24}$ H cm^{-2} (Lis & Goldsmith 1989). Thus the sources well outside the (1–10)$\times 10^{23}$ H cm^{-2} range should be regarded as either background AGNs or foreground stars. No. 2 and 5 show the $N_{\rm H}$ of $< 1 \times 10^{23}$ H cm^{-2} within the error, hence are regarded as foreground stars. The others are likely located in the cloud (hereafter, the cloud members).

Since the statistics of individual cloud member is limited (6–80 photons, see Table 2), we group them into two classes; class A comprises No. 10–13, which are associated with the HII regions, and the class B sources have neither radio nor IR counterpart (No. 1, 3, 4, 6–9, and 14–17). We then make the composite spectra for the class A and B sources (Figure 3) separately, and examine the average properties.

The composite spectra are nicely fitted with a thin thermal plasma of solar-abundances. However, an excess near at 6.4 keV is found, hence we add a narrow line at 6.4 keV, which represents the K-shell transition of neutral or low-ionization irons. The best-fit parameters and models are shown in Table 1 and Figure 3, respectively. The mean $N_{\rm H}$ of 3.6 and 1.3 $\times 10^{23}$ H cm^{-2} for the class A and B sources are consistent with being in the cloud.

For the spectral fitting of individual X-ray sources, allowable (free) parameters depend on the continuum and line fluxes. Since No. 10 shows the strong iron lines (see Figure 4) and the total flux is reasonably high (51 counts), we allow the temperature (kT), absorption column density ($N_{\rm H}$), abundance (Z), and equivalent width ($E.W.$) of the 6.4-keV line to be free. For comparison, we also use the same free parameters for No. 13. For the other sources, we refer the best-fit parameters of the composite spectra with free parameters depending on the flux; those with flux between 29–50 counts (No. 8 and 11), free parameter is $N_{\rm H}$; and the faintest sources less than 21 counts, we fix all the parameters to those of the composite spectra and estimate the luminosity ($L_{\rm x}$) only. The best-fit thin thermal plasma model parameters are listed in Table 2, while the spectra and the best-fit models of the two brightest sources, No. 10 and 13, are shown in Figure 4.

Since the 6.4-keV line feature in addition to the 6.7-keV line may be sensitive to the charge transfer inefficiency (CTI), we examine the CTI correction issue using the software described by the method of Townsley et al. (2001). In order to achieve the best statistics, we use the diffuse emission from all the $3' \times 3'.5$ region which includes the strong 6.4-keV line in Sgr B2 (Murakami et al. 2001). The standard level 2 process gives the center energy of 6.40 (6.36 − 6.41) keV, flux of 5.6 (5.1 − 6.2) $\times$ 10^{-5} photons cm^{-2} s^{-1}, and width of 60 (8.8 − 130) eV, which are essentially the same as those by the method of Townsley et al. (2001) (see Table 2 in Murakami et al. 2001). Thus we conclude that the Level 2 process correct the CTI reasonably well, at least for the present data set.

The 6.4-keV line flux is also sensitive to the background subtraction, because the background itself is a luminous 6.4-keV line source. We therefore re-subtract the background taken from the right half region of Sgr B2, where the 6.4-keV line is about two times larger than the average. Still we obtain consistent results. Thus the 6.4- and 6.7-keV iron lines are not artifacts due to CTI nor background subtraction.

We examine the time variability for all sources with the Kolmogorov-Smirnov test (Press et al. 1992) under the constant flux hypothesis using *lcstats* in the **XRONOS** (Ver 5.16) package[3]. Five (cloud members) and two (non cloud members) sources are found to be time variable with more than 90 % significant level. However, no flare-like event

[3]see http://xronos.gsfc.nasa.gov

with a fast rise and slow decay profile is found from any of them.

3. Discussion

3.1. X-rays Associated with the HII complexes

No. 10 and 13, the most obvious cloud members, are associated with the complex of ultra compact HII regions (UC HIIs), Sgr B2 (M) (e.g., Gaume & Claussen 1990) (see Figure 2). The absorption column density of $\sim 4 \times 10^{23}$ H cm^{-2} supports that No. 10 and No. 13 are lying in the core of the Sgr B2 (M).

No. 10 seems to be elongated along the UC HIIs F3, F4 and G (De pree et al. 1998) and the MIR source MSX5C G000.6676-00.0355 (Egan et al. 1999), hence would comprise several point sources. The X-ray peak comes near the position of the brightest UC HII, F3 (De Pree et al. 1998), which is also considered to be an engine of the HC_3N bipolar flow (Lis et al. 1993). From the HII and outflow data, this X-ray peak may correspond to a very high-mass (e.g., O6, assuming the zero age main sequence (ZAMS) star: De Pree et al. 1998), young (well below 10^5 year: Lis et al. 1993) star.

A notable feature of No. 10 is strong lines at 6.7 keV and 6.4 keV. The best-fit iron abundance of 5 times of solar is extremely large but, within the large error, it is consistent with that of the Sgr B2 cloud of 2–3, estimated from X-ray reflection nebula (Murakami et al. 2001) and that predicted from the abundance gradient of HII regions toward the GC (e.g., Simpson et al. 1995). The abundances, on the other hand, is significantly larger than that of any other high-mass SFRs (Kohno et al. 2002; Schulz et al. 2001; Yamauchi et al. 1996). It may be noted that He66α line observation by De Pree et al. (1996) predicts anomalously low helium-abundance from the HII region F only, in contrast of apparent iron overabundance with the present study.

No. 13 is also extended, lying beyond the east filament of the cometary HII region I (Gaume & Claussen 1990). The ionized gas filament is likely produced by an interaction of outflow(s) from the UC HIIs F as is supported by the extremely broad H66α recombination lines (De Pree et al. 1996). However the outflow velocity of $\sim$ 100 km s^{-1} (FWHM of the line width; Gaume et al. 1995) is insufficient to produce the 5-keV plasma we observed.

The best-fit iron abundance of No. 13, in contrast to No. 10, is sub-solar (0.3 of solar), although the error is large for a concrete conclusion. It is debatable whether the chemical abundances or the X-ray emission mechanisms is different between the two sources (No 10 and 13) in Sgr B2 (M) separated by only 0.2–0.3 pc.

No. 11 is extended over the whole region of Sgr B2 (N). The best-fit absorption of 5.7×10^{23} H cm^{-2} supports that No. 11 is located in the core of the UC HII complex. The radio continuum and molecular bipolar flow data indicate that Sgr B2 (N) is younger than Sgr B2 (M) (Gaume et al. 1995; Lis et al. 1993) and may contain $\sim$ 7 massive stars ranging from O5 to B0 (Gaume et al. 1995). The He66α line from one of the UC HII (K6) in Sgr B2 (N) shows doubly peaked profile, indicating an expanding shell of the dynamical age of $\sim 10^4$ year (De Pree et al. 1995). From the expansion velocity of $\sim$ 22 km s^{-1} (De Pree et al. 1995), this shell can not be an origin of the hard X-rays of No. 11.

No. 12, at the Sgr B2 (S), is not resolved, and is likely to associated with an isolated star of spectral type O6.5 (Gaume et al. 1995). The MIR source MSX5C G000.6564–00.0411 is also found at No. 12 within 1σ position error (Egan et al. 1999).

3.2. Origin of the X-rays from the HII Regions

As we discussed in the previous sections, X-ray sources No. 10–13 are closely associated with the UC HII complexes Sgr B2 (M), (N) and (S) with the absorption corrected luminosity (in 2–10 keV) of 23, 12 and 2.2×10^{32} erg s^{-1}, respectively. Since Sgr B2 (M), (N) and (S) may contain $\sim$ a few to 20 UC HIIs each (De Pree et al. 1998), No. 10–13 are possibly clusters of high-mass YSOs with similar numbers. The individual YSO luminosity is then $\sim 10^{32}$ erg s^{-1}, which is consistent with the high-mass YSOs (Kohno et al. 2001; Schulz et al. 2001).

The plasma temperatures of about 5 keV are, however, significantly higher than that of stellar-wind-driven X-rays found in high-mass main sequence stars (MSSs) (Berghöfer et al. 1997). We accordingly propose a scenario that high-mass

stars produce hard ($\geq$5 keV) X-rays due to the magnetic activity in a phase of pre main sequence (Babel & Montnerle 1997; Hayashi, Shibata, & Matsumoto 1996). In fact, high temperature plasma has been found from high-mass YSOs in the Orion Nebula and Mon R2 cloud (e.g., Shultz et al. 2001; Kohno et al. 2001). It may continue until ZAMS, then gradually decline to the stellar wind dominant activity. Finally, high-mass MSSs predominantly emit soft ($\leq$1 keV temperature) X-rays originated from the strong stellar wind.

The observed temperature of about 5 keV is, on the other hand, more typical to low-mass protostars (Kamata et al. 1997; Koyama et al. 1996a; Tsuboi et al. 2000; Imanishi, Koyama, & Tsuboi 2001) with the luminosity of $\sim 10^{28-30}$ erg s^{-1} (Feigelson et al. 1993; Casanova et al. 1995), hence it is also possible that No. 10–13 is a cluster of numerous number (10^2–10^4) of low-mass YSOs. The most probable scenario, therefore, would be that the X-rays from the UC HII complexes are the mixture of YSOs with various mass range (high-medium-low mass stars).

The best-fit absorption of $\sim 5 \times 10^{23}$ H cm^{-2} for the Sgr B2 (M) X-rays is the largest among the known stellar X-ray sources. Our observation demonstrates that hard X-rays are very powerful to discover deeply embedded YSOs even if they are suffered with a large optical extinction of $Av\sim$200–300 mag.

3.3. X-ray sources with no HII region (class B)

In the Sgr B2 cloud, we find 11 class B sources. The lowest flux of those sources is estimated to be 3×10^{-15} erg cm^{-2} s^{-1} after removing the absorption of 1.3×10^{23} H cm^{-2}, the mean value of the class B sources. The expected number of extra galactic sources above the flux of 3×10^{-15} erg cm^{-2} s^{-1} is only $\sim$ 2.5 in the Sgr B2 region of $3' \times 3'.5$ (Mushotzky et al. 2000). If we fit the composite class B spectrum with a power-law model, the photon index is found to be $\Gamma < 1.3$, which is out side of the typical value for AGNs (1.5–2.0). The average $N_{\rm H}$ of 1.3×10^{23} H cm^{-2} also supports that most of the class B sources are not background AGNs, but are the cloud members. The temperature of $>$ 4.2 keV (see Table 1), and each X-ray luminosity of a few times 10^{31-32} erg s^{-1} are consistent with those of class A sources, hence support that the class B source is either a single or cluster of YSO(s) with various mass ranges. The time variable sources is likely a single star, either a high-mass or a low-mass in the high end of the luminosity function.

A problem of the YSO scenario is that no HII region, maser source, nor outflow has been found. Furthermore, the star forming regions and high density regions elongate north to south in Sgr B2 (e.g., Sato et al. 2000), while the class B sources are widely distributed over the whole Sgr B2 cloud. This leads us to an alternative scenario that isolated white dwarfs (WDs) are powered by the Bondi-Hoyle accretion (Bondi & Hoyle 1944) from the dense cloud gas. In fact, the observed thin thermal plasma with the mean temperature of $>$ 4.2 keV is consistent with those of accretion powered WDs (e.g., Ezuka & Ishida 1999 and references there in). The Bond-Hoyle accretion rate is given by;

$$\dot{M} = 2\times10^{15} \left(\frac{n_{\rm H_2}}{10^4 \text{ cm}^{-3}}\right) \left(\frac{v}{10 \text{ km s}^{-1}}\right)^{-3} \left(\frac{M}{M_\odot}\right)^2 \text{g s}^{-1}, \quad (1)$$

where M and v are the mass and traveling velocity of WDs relative to cloud, and $n_{\rm H_2}$ is the number density of molecular hydrogen in the cloud. The mean $n_{\rm H_2}$ can be estimated to be $\sim 10^4$ cm^{-3}, from the $N_{\rm H}$ value of 10^{24} H cm^{-2} and typical depth of the cloud of about 20 pc (Lis & Goldsmith 1989). The X-ray luminosity is given by $L_{\rm x} = GM\dot{M}/R$, where R is the radius of the WD and G is the gravitational constant. Assuming the standard mass to radius relation of WDs ($R = 5.5 \times 10^8 (M/M_\odot)^{-1/3}$), $L_{\rm x}$ is estimated

$$L_{\rm x} = 10^{32} \left(\frac{n_{\rm H_2}}{10^4 \text{ cm}^{-3}}\right) \left(\frac{v}{10 \text{ km s}^{-1}}\right)^{-3} \left(\frac{M}{0.6\ M_\odot}\right)^{10/3} \text{erg s}^{-1}, \quad (2)$$

where, 0.6 $M_\odot$ is the typical mass of WDs (Ramsay 2000 and references there in). Accordingly, with a reasonable range of gas density and WD parameters, the predicted X-ray luminosity is consistent with that of the observations. The number density of WDs in the solar neighbor is (5–6)$\times 10^{-3}$ pc^{-3} (Holberg, Oswalt, & Sion 2001). Since the number density of stars near the Sgr B2 region (100 pc from the GC) is more than 10^2 times higher than that the solar neighbor (e.g., Oort 1977), the population of WDs in our observed area (assuming a rectangle of $7.2 \times 8.4 \times 20$ pc^3)

can be estimated to be > 600. Therefore it is conceivable that the class B sources are a part of isolated WDs, which may lie in the higher end of the luminosity function.

3.4. Cloud Cores Irradiated by X-ray Sources

The composite spectra of all the cloud members has a 6.4-keV line with the *E.W.* of 200–230 eV. The line energy corresponds to the K-shell emission from neutral or low-ionized irons, hence the most plausible origin is fluorescence from cold irons in the cloud gas. Assuming that homogeneous circumstellar gas is irradiated by a central X-ray sources, the required column density to emit observed 6.4 keV line is estimated from the relation of,

$$E.W. \sim 100\ Z_{\rm Fe}\ (\frac{N_{\rm H}}{10^{23}\ {\rm H\ cm^{-2}}})\ {\rm eV}, \qquad (3)$$

where $Z_{\rm Fe}$ is the iron abundance relative to solar (Inoue 1985). Most of the source photons (except for No. 11) are extracted from a circle with a 3×HPD-diameter, which corresponds ~ 0.1 pc in radius. Thus the number density of atomic hydrogen ($n_{\rm H}$) in the source regions must be $6{\times}10^5$ cm^{-3}, assuming $Z_{\rm Fe}$ is 1. This estimated value exceeds the average $n_{\rm H_2}$ in the Sgr B2 cloud of $\sim 10^4$ cm^{-3} (see previous subsection). We further find that the *E.W.* does not decrease as we reduce the radius of the photon extraction circles. Therefore the gas density should be concentrated very close to the X-ray sources. In fact, De Pree et al. (1998) suggested that the density ($n_{\rm H_2}$) in the close vicinity ($\sim 10^{-3}$ pc) of the UC HII region in Sgr B2 (M) is in between $2 \times 10^7{\rm cm^{-3}}$ and $1 \times 10^8{\rm cm^{-3}}$, if they are in pressure equilibrium.

No. 10 requires exceptionally strong 6.4-keV line with the *E.W.* of 630 eV. Using the $n_{\rm H_2}$ value proposed by De Pree et al. (1998) and the core radius of 10^{-3} pc, the column density in the core region of Sgr B2 (M) is (1–6)$\times 10^{23}$ H cm^{-2}. Then the expected abundance $Z_{\rm Fe}$ is $\sim$ 1–6, which is consistent with the best-fit value of a thin thermal fit (see 3.1).

The X-ray sources in a dense cloud cores such as Sgr B2 (M), (N), and (S), may photo-ionize the core regions. Using the X-ray ionization rate by Lorenzani & Palla (2001), we estimate that a dense core of $n_{\rm H} \sim 10^{7-8}$ cm^{-3} is largely ionized within $\sim 0.01 - 0.03$ pc in radius from a central source of 10-keV plasma with the luminosity of 10^{32} erg s^{-1}. For Sgr B2 (M), which may contains ~ 20 X-ray sources in a ~ 0.15-pc radius, the ionized volume is $\sim 1 - 20\%$ of the core. Since the ionized gas strongly couples to the magnetic field, it may have a significant effect on the cloud compression for star formation.

The X-ray ionization may also have an impact on the abundance of molecules. The abundance of HC_3N, for example, drops very rapidly with increasing ionization. The HC_3N abundance in Sgr B2 (M) is 20 times less than that of Sgr B2 (N) (De Vicente et al. 2000). Since Sgr B2 (N) is less X-ray active and more largely extended than Sgr B2 (M), the abundance difference between these two cloud cores may be explained with the X-ray ionization effect.

4. Conclusion

1. We discovered a dozen X-ray sources in the giant molecular cloud Sagittarius B2 (Sgr B2). Judging from the large absorptions ($N_{\rm H}$) of (1–10)$\times 10^{23}$ H cm^{-2} and log$N$-log$S$ relation for the background sources, most of these are the cloud members.

2. The brightest two sources are found near at the HII complex Sgr B2 (M), which are likely the cluster of X-ray emitting YSOs. The X-ray spectra are largely different between the two sources. One has extremely strong iron lines, while the other has only weak lines.

3. X-ray excess from the HII complexes Sgr B2 (N) and (S) are found, the former is extended, while the latter is point-like. Both have the X-ray spectra and luminosities consistent with YSOs. No significant X-rays are found from any other HII regions.

4. The other X-ray sources also have the X-ray spectra and luminosities consistent with a single or a cluster of YSO(s). However, no counterpart of any other wavelength, neither optical/IR star, HII region, maser source nor molecular core has been reported. Thus alternative possibility is isolated white dwarfs powered by the Bondi-Hoyle accretion.

5. Strong 6.4-keV lines are found from the X-ray sources. The origin of this line would be the fluorescence of the circumstellar gas irradiated by the central stars. The gas density is not uniform but is centrally concentrated.

We thank to our referee, E. Feigelson for his useful comments and suggestions. H. M. is financially supported by the Japan Society for the Promotion of Science.

REFERENCES

Babel, J. & Montmerle, T. 1997, A&A, 323, 121

Benson, J. M. & Johnston, K. J. 1984, ApJ, 277, 181

Berghöfer, T. W., Schmitt, J. H. M. M., Danner, R., & Cassinelli, J. P. 1997, A&A, 322, 167

Bondi, H. & Hoyle, F. 1944, MNRAS, 104, 273

Casanova, S., Montmerle, T., Feigelson, E.D., & André, P. 1995, ApJ, 439, 752

De Pree, C. G., Gaume, R. A., Goss, W. M., & Glaussen, M. J. 1995, ApJ, 451, 284

De Pree, C. G., Gaume, R. A., Goss, W. M., & Glaussen, M. J. 1996, ApJ, 464, 788

De Pree, C. G., Goss, W. M., & Gaume, R. A. 1998, ApJ, 500, 847

De Vicente, P., Martín-Pintado, J., Neri, R., & Colom, P. 2000, A&A, 361, 1058

Egan, M. P., Price, S. D., Shipman, R. F., Gugliotti, G. M., Tedesco, E. F., Moshir, M., & Cohen, M. 1999, ASP Conf. Ser. 177: Astrophysics with Infrared Surveys: A Prelude to SIRTF, 404

Ezuka, H., Ishida, M. 1999, ApJS, 120, 277

Feigelson, E. D., Casanova, S., Montmerle, T., Guibert, J. 1993, ApJ, 416, 623

Feigelson, E. D. & Montmerle, T. 1999, ARA&A, 37, 363

Garmire, G., Feigelson, E. D., Broos, P., Hillenbrand, L. A., Pravdo, S. H., Townsley, L., & Tsuboi, Y. 2000, AJ, 120, 1426

Garmire, G. P., Nousek, J. P., & Bautz, M. W. 2001, in preparation

Gaume, R. A. & Claussen, M. J. 1990, ApJ, 351, 538

Gaume, R. A., Claussen, M. J., De Pree, C. G., Goss, W. M., & Mehringer, D. M. 1995, ApJ, 449, 663

Goldsmith, F. P., Lis, D. C., Lester, D. F., & Harvey, P. M. 1992 ApJ, 389, 338

Hayashi, M. R., Shibata, K., & Matsumoto, R. 1996, ApJ, 468, L37

Høg, E., Abricius, C., Makarov, V. V., Urban, S., Corbin, T., Wycoff, G., Bastian, U., Schwekendiek, P., & Wicenec, A. 2000, A&A, 355, 27

Holberg, J. B., Oswalt, T. D., & Sion, E. M. 2001, in ASP conf. ser. 226, Proc. 12th European Workshop White Dwarfs, ed. Provencal, J. L., Shipman, H. L., MacDonald, J., & Goodchild, S. (San Fransisco: ASP), 375

Imanishi, K., Koyama, K., & Tsuboi, Y. 2001, ApJ, 557, 747

Inoue,H. 1985, Space Sci. Rev., 40, 317

Kamata, Y., Koyama, K., Tsuboi, Y., & Yamauchi, S. 1997, PASJ, 49, 461

Kobayashi, H., Ishiguro, M., Chikada, Y., Ukita, N., Morita, K.-I., Okumura, S. K., Kasaga, T., & Kawabe, R. 1989, PASJ, 41, 141

Kohno, M., Koyama, K., & Hamaguchi, K. 2002, ApJ, (in press)

Koyama, K., Hamaguchi, K., Ueno, S., Kobayashi, N., & Feigelson, E. D. 1996a, PASJ, 48, 87

Koyama, K., Maeda, Y., Sonobe, T., Takeshima, T., Tanaka, Y., & Yamauchi, S. 1996b, PASJ, 48, 249

Kuan, Y. -J. & Snyder, L. E. 1996, ApJ, 470, 981

Lis, D. C. & Goldsmith, P. F. 1989, ApJ, 337, 704

Lis, D. C., Goldsmith, P. F., Carlstrom, J. E., & Scoville, N. Z. 1993, ApJ, 402, 238

Liu, S. Y., Mehringer, D. M., Miao, Y., & Smyder, L. E. 1998, ApJ, 501, 680

Lorenzani, A. & Palla, F. 2001, in ASP conf. ser. 243, Darkness to Light, ed. Montmerle, T. & André, Ph. (San Fransisco: ASP), 745

Mehringer, D. M., Goss, W. M., & Palmer, P. 1994, ApJ, 434, 237

Mehringer, D. M. 1995, ApJ, 454, 782

Montmerle, T., Grosso, N., Tsuboi, Y., & Koyama, K. 2000, ApJ, 532, 1097

Murakami, H., Koyama, K., & Maeda, Y. 2001, ApJ, 558, 687

Mushotzky, R. F., Cowie, L. L., Barger, A. J., & Arnaud, K. A. 2000, Nature, 404, 459

Oort, J. H. 1977, ARA&A, 15, 295

Press, W.H., Teukolsky, S.A., Vetterling, W.T., & Flannery, B.P. 1992, Numerical Recipes in C (2nd ed; London: Cambridge University Press)

Ramsay, G. 2000, MNRAS, 314, 403

Reid, M. J., Schneps, M. H., Moran, J. M., Gwinn, C. R., Genzel, R., Downes, D., & Rönnäng, B. 1988, ApJ, 330, 809

Sakano, M. 2000, Ph. D. thesis, Kyoto University

Sato, F., Hasegawa, T., Whiteoak, J. B., & Miyawaki, R. 2000 ApJ, 537, 857

Schulz, N.S., Canizares, C., Huenemoerder, D., Kastner, J. H., Taylor, S. C., & Bergtrom, E. J. 2001, ApJ, 549, 441

Shiki, S., Ohishi, M., & Deguchi, S. 1997, ApJ, 478, 206

Simpson, J. P., Colgan, S. W. J., Rubin, R. H., Erickson, E. F., & Haas, M. R. 1995, ApJ, 444, 721

Townsley, L. K., Broos, P. S., Garmire, G. P., & Nousek, J. A. 2000, ApJ, 534, 139

Tsuboi, Y., Imanishi, K., Koyama, K., Grosso, N., & Montmerle, T. 2000, ApJ, 532, 1089

Vogel, S. N., Genzel, R., & Palmer, P. 1987, ApJ, 316, 243

Weisskopf. M. C., O'dell, S., & van Speybroeck, L. P., 1996, Proc. SPIE, 2805, 2

Yamauchi, S., Koyama, K., Sakano, M., & Okada, K. 1996, PASJ, 48, 719

This 2-column preprint was prepared with the AAS LaTeX macros v5.0.

TABLE 1
BEST-FIT RESULTS OF THE COMBINED SPECTRA

class	$N_{\rm H}$ (1)	kT (2)	Z (3)	$E.W.$ (4)	$L_{\rm X}$ (5)	Reduced χ^2 $(d.o.f)$
A	3.6 (2.8–4.5)	6.5 (2.9–13)	1.0 (fixed)	200 (< 420)	33 (26–38)	0.6 (9)
B	1.3 (0.93–1.8)	9.5 (>4.2)	1.0 (fixed)	230 (< 480)	15 (13–17)	1.0 (8)

NOTE.—Parentheses indicate the 90% confidence limit. (1):absorption column density of hydrogen (10^{23} H cm^{-2}). (2):plasma temperature (keV). (3):abundance (solar ratio). (4) equivalent width (eV) of the 6.4-keV line (Fe K_α of neutral iron). (5):absorption corrected luminosity in 2–10 keV (10^{32} erg s^{-1}).

TABLE 2

Chandra X-RAY SOURCES IN THE SGR B2 CLOUD

No.	R.A. (J2000)	Dec. (J2000)	Cts (1)	Var. (2)	$N_{\rm H}$ (3)	kT (4)	Lx (5)	Z (6)	$E.W.$ (7)	counterpart (8)	size (9)
1	17:47:13.6	−28:23:37.8	19	···	–[†]	–	0.83 (0.51–1.2)	–	–	···	2.″38
2	17:47:14.1	−28:23:31.1	13	> 99.9	0.56[⋆] (0.34–0.90)	···	(5.7[⋆⋆] (4.1–7.3))	···	···	(foreground)	2.″59
3	17:47:15.1	−28:24:41.6	7.2	···	–	–	0.40 (0.14–0.65)	–	–	···	1.″65
4	17:47:15.5	−28:21:40.8	15	99.2	–	–	1.2 (0.68–1.7)	–	–	···	5.″44
5	17:47:15.8	−28:24:17.1	18	> 99.9	0.082[⋆] (0.059–0.11)	···	(3.8[⋆⋆] (2.9-4.7))	···	···	(foreground)	2.″01
6	17:47:16.4	−28:21:32.2	18	···	–	–	0.83 (0.50–1.2)	–	–	···	6.″00
7	17:47:17.2	−28:24:09.2	12	99.5	–	–	0.50 (0.25–0.75)	–	–	···	2.″40
8	17:47:18.2	−28:23:48.7	41	···	0.78 (0.49–1.4)	–	2.2 (1.5–2.7)	–	–	···	3.″00
9	17:47:20.1	−28:24:16.9	14	96.6	–	–	0.65 (0.35–0.94)	–	–	···	2.″96
10	17:47:20.2	−28:23:05.3	51	···	4.0 (1.9–8.8)	10 (4.1–30)	8.7 (4.3–17)	5.0 (>0.94)	630 (180–1100)	Main	4.″24
11	17:47:20.3	−28:22:15.3	29	···	5.7 (>1.8)	–	12 (5.3–18)	–	–	North	25.″0 × 21.″0[*]
12	17:47:20.4	−28:23:45.4	12	···	–	–	2.2 (1.1–3.3)	–	–	South	4.″00
13	17:47:20.9	−28:23:06.2	83	···	3.8 (2.3–7.2)	5.1 (>1.1)	14 (11–18)	0.31[‡]	62 (<370)	Main	5.″20
14	17:47:22.3	−28:23:26.4	15	95.6	–	–	1.4 (0.79–2.0)	–	–	···	4.″35
15	17:47:23.1	−28:22:32.4	20	91.0	–	–	1.3 (0.81–1.8)	–	–	···	5.″72
16	17:47:23.2	−28:23:25.3	6.0	···	–	–	0.26 (0.080–0.44)	–	–	···	4.″59
17	17:47:23.8	−28:22:31.7	6.0	···	–	–	0.66 (0.20–1.1)	–	–	···	6.″00

NOTE.— Parentheses indicate the 90% confidence limit. Col. (1):photon counts (background subtracted). Col. (2):variability of more than 90 % confidence level is given with the Kolmogorov-Smirnov test. Col. (3):absorption hydrogen column density (10^{23} H cm^{-2}). Col. (4):plasma temperature (keV). Col. (5):absorption corrected luminosity in 2–10 keV (10^{32} erg s^{-1}). Col. (6):abundance relative to solar value. Col. (7):equivalent width (eV) of the 6.4-keV line (Fe K_α of neutral iron). Col. (8):counterpart of HII complexes (No. 10–13). Col. (9):the radius of photon extracted circle.

[†]: Hyphen (–) means the fixed value to the best-fit parameters of the composite spectra (see Table 1). [‡]:Errors are not constrained. [⋆]: The fitting model is a 1-keV thin thermal plasma of solar abundance. [⋆⋆]: absorption corrected X-ray flux in 2–10 keV (10^{-15} erg cm^{-2} s^{-1}). [*]: The source region is rectangle.

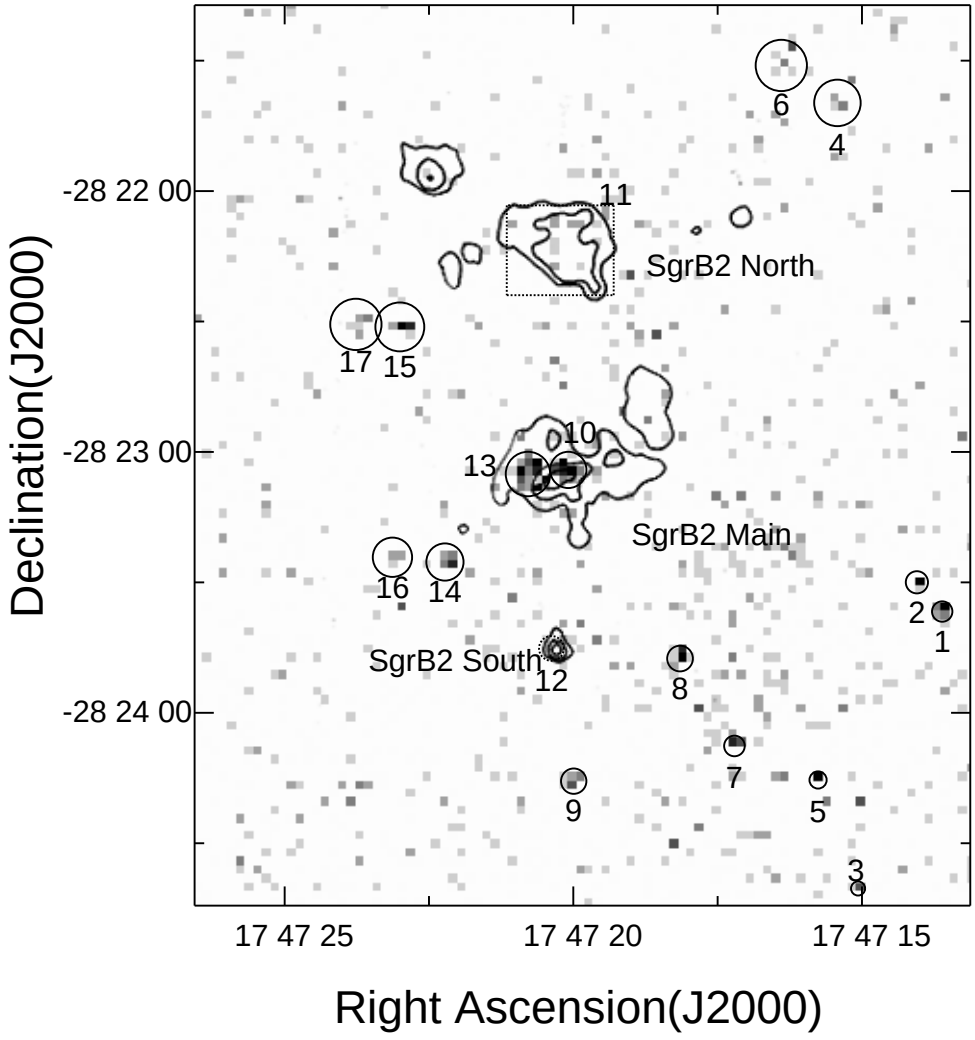

Fig. 1.— The 2–10keV X-ray band image of Sgr B2, overlaid on contours of HII regions (Gaume et al. 1995). The bin size is $1'' \times 1''$ (2×2 pixels are summed). The solid circles and dotted area (box: No. 11, circle: No. 12) indicate the source regions for the X-ray sources detected with '*wavdetect*' and manually , respectively (see text).

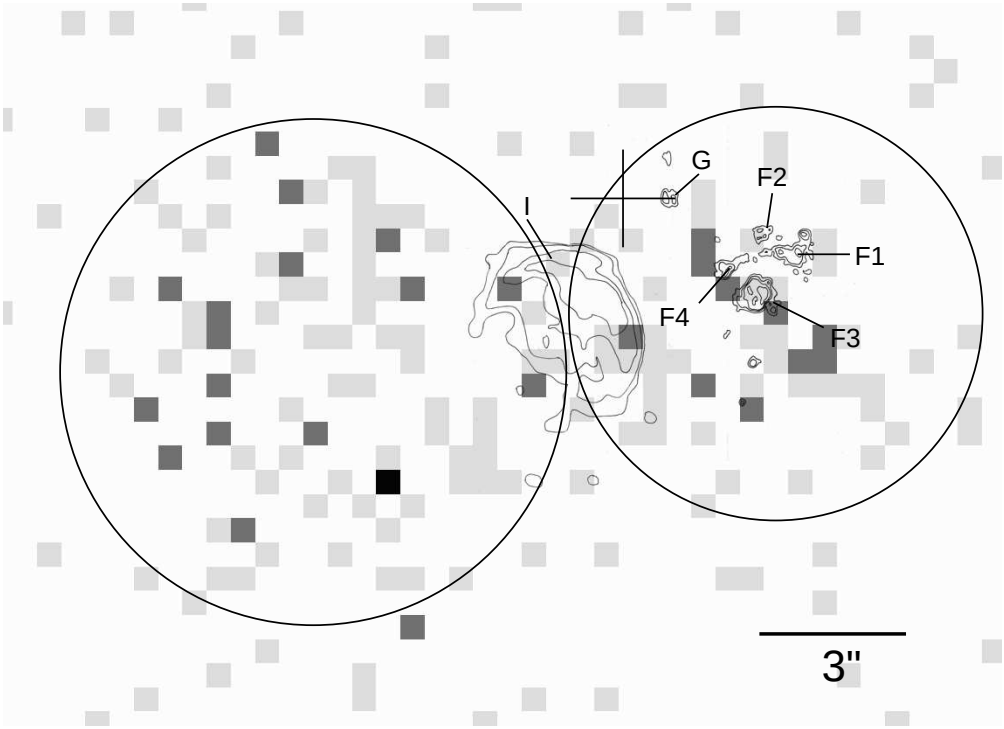

Fig. 2.— The 2–10 keV band X-ray image. near Sgr B2 (M), overlaid on the contours of HII regions F1–F4, G (De Pree et al. 1998), and I (Gaume & Claussen 1990). The bin size is $0.''5 \times 0.''5$. The cross (+) indicates the position and 1σ errors ($\sim 1.''1$) of the MIR source MSX5C G000.6676-00.0355. The right source is No. 10, and the left source is No. 13. The X-ray spectra (see Figure 4) are obtained from the solid circle regions (see text).

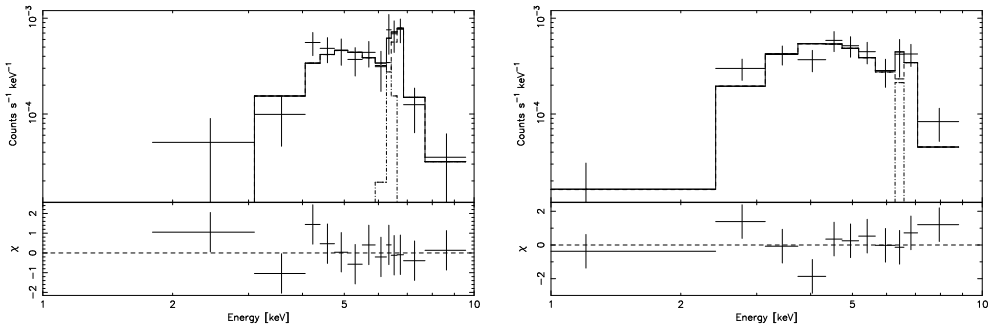

Fig. 3.— The composite X-ray spectra of the class A (left) and B (right) sources and the best-fit model of a thin thermal plasma (solid histogram) with a 6.4-keV line (dotted histogram). X-ray photons are extracted either from the box (for No. 11) or circles (the other sources) with a diameter of 3×HPD (see Figure 1).

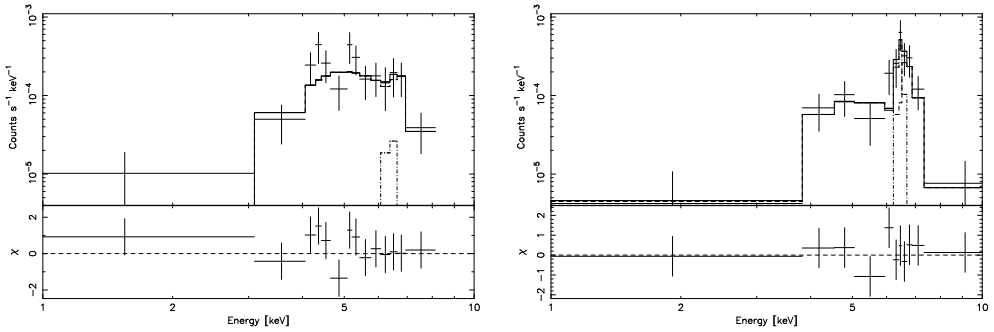

Fig. 4.— The X-ray spectrum and the best-fit model of a thin thermal plasma (solid histogram) with a 6.4-keV line (dotted histogram) for sources No. 13 (left) and No. 10 (right).